NANO LETTERS

2008
Vol. 8, No. 7
1923-1928

Inverted Size-Dependence of Surface-Enhanced Raman Scattering on Gold Nanohole and Nanodisk Arrays

Qiuming Yu,*[,†,‡] Phillip Guan,[‡,§] Dong Qin,[†,‡,⊥] Greg Golden,[†,‡,¶] and Paul M. Wallace[†,‡]

Department of Chemical Engineering, Center for Nanotechnology, and Department of Bioengineering, University of Washington, Seattle, Washington 98195

Received February 29, 2008; Revised Manuscript Received June 4, 2008

ABSTRACT

Surface-enhanced Raman scattering (SERS) on gold nanohole and nanodisk arrays with precisely controlled size and spacing fabricated via electron beam lithography was investigated. These nanostructures exhibit strong SERS signals at 785 nm excitation but not at 514 nm. When the edge-to-edge distance is maintained, enhancement increases for nanoholes but decreases for nanodisks as diameter is increased. It is shown that the observed enhancement results from the local surface plasmon resonance wavelength shifts to the near-infrared regime as nanohole diameter increases. The large tolerance on dimensions and the empty space confined by nanoholes suggest promise for their use as a functional component in sensing, spectroscopy, and photonic devices.

The optical properties of noble metal thin films with subwavelength hole structures has spurred great interest recently because of their potential applications in novel photonic devices and biosensors.[1,2] It has been shown that the highly unusual transmission efficiency of light through subwavelength hole arrays in a metal film is due to the coupling of light with surface plasmons on the periodically patterned metal film.[3,4] The conservation of quantum entanglement for the conversion from photon to surface plasmon to photon through such nanostructure metal optical elements demonstrates that surface plasmons have a true quantum nature.[5] The dependence of these unusual optical properties on the parameters such as diameter, shape, and orientation of holes as well as periodicity, thickness, and type of metal thin film has also been studied experimentally[2,3,6,7] and theoretically.[8–10] Recent experimental[11] and theoretical[8,12] studies have demonstrated that strong localized surface plasmon resonances (LSPR) are associated with individual or short-range ordered nanometer-sized holes in metal films,[8,11,13–15] which are qualitatively similar to dipolar local surface plasmon excitations in gold nanodisks. These nanohole structures were also used in detecting lipid-membrane mediated biorecognition events[14] and the adsorption of different chain length alkane thiols and proteins[16,17] as substrates in prototype LSPR biosensors. The sensitivity of LSPR sensors based on nanohole structures was found to be 400 nm per refractive index unit, which is comparable to other grating-based surface plasmon resonance (SPR) devices.[18] While the optical properties enhanced by surface plasmon observed in metal nanohole structures and its application as LSPR sensors are new, the LSPR associated with metal nanoparticles synthesized chemically[19,20] or fabricated by nanosphere lithography (NSL)[21] or colloidal lithography[22,23] or electron beam lithography (EBL)[24] and their applications in biosensors[25] has been studied extensively. The theoretical and experimental studies of the geometric effect of holes and particles on localized surface plasmons were reviewed recently.[26]

Surface-enhanced Raman scattering (SERS) is another phenomenon strongly dependent on the dipolar surface plasmon excitations of metal nanostructures. The significantly increased intensity of Raman scattering from vibrational bands of a molecule at or near a nanostructured surface is due to extremely high local electromagnetic fields associated with LSPR.[27] For chemically synthesized nanoparticles[19,20] or fabricated nanoparticle arrays,[24,28–31] it was found that the wavelength of LSPR was related to the size and shape of particles and the spacing between them, which in turn affected the intensity of the SERS signal. The maximum Raman enhancement is obtained for an LSPR located between the irradiation wavelength, λ_{ex}, and the molecule vibration band wavelength, λ_{vib}.[19,28,30,32] By using nanofab-

* Author to whom correspondence should be addressed. E-mail: qyu@u.washington.edu. Phone: 206-543-5101. Fax: 206-221-2528.
† Department of Chemical Engineering.
‡ Center for Nanotechnology.
§ Department of Bioengineering.
⊥ Current address: School of Engineering, Washington University, St. Louis, MO.
¶ Current address: NanoMaterials Discovery, Seattle, WA.

10.1021/nl0806163 CCC: $40.75
Published on Web 06/19/2008

rication tools such as electron beam lithography, one can rationally design and precisely control the size and shape of nanostructures and the distance between them. Therefore, the wavelength of LSPR can be tuned in order to optimize the SERS spectroscopy. Recently, nanohole-enhanced Raman scattering from the subwavelength nanohole arrays in ultrathin gold[33] and silver[34] films have been investigated as a function of lattice spacing. It was found that the enhancement of Raman signals was associated with plasmons localized near the edge of holes. However, comparison between experiment and theory from silver nanohole arrays demonstrated that the enhancement from localized plasmons associated with the nanoholes is about 3 orders of magnitude lower than that from nanometer scale roughness associated with the silver film in the absence of nanoholes.[34]

In this communication, we report a systematical study of SERS on gold nanohole arrays with controlled diameter, 40−520 nm, and edge-to-edge distance, 60−120 nm, fabricated by EBL and compare the results with SERS on gold nanodisk arrays with comparable geometric parameters. We show that 4-mercaptopyridine adsorbed on gold nanohole arrays exhibits SERS spectra and the intensity of SERS spectra increases significantly as nanohole diameter is increased. An opposite trend of SERS signals as a function of diameter is observed on nanodisk arrays. Collected normal incidence transmission spectra show that the LSPR wavelength is shifted toward the near-infrared regime as the diameter of nanoholes is increased.

By using an FEI Sirion scanning electron microscope (SEM) equipped with Nabity NPGS software, 20 μm × 20 μm gold nanohole and nanodisk arrays with a square grid of different diameters and spaces (dimensions can be found in Table 1 in Supporting Information) were fabricated by EBL. A layer of 100 nm thick polymethyl methacrylate (PMMA) electron-sensitive resist was spin-coated on a 20 nm gold coated silicon substrate and exposed to the 16.5 pA electron beam with a line dose in the range of 0.3−0.7 nC/cm. Nanoholes were generated in PMMA layer after development in 1:3 methyl isobutyl ketone/isopropanol (MIBK/IPA) PMMA developer for 70 s, followed by IPA rinse and post bake at 95° for 30 min. The gold nanohole arrays were created by evaporating 2 nm Cr and 50 nm gold film to the PMMA surface as illustrated in Figure 1a. On these nanohole array substrates, a physically separated layer of isolated gold disks exists at the bottom of the well. The gold nanodisk arrays as illustrated in Figure 2a were prepared by following the same procedure as described previously with an additional step of gold lift-off accomplished by immersing the substrate in acetone. Another set of nanohole arrays was prepared on an ITO glass substrate coated with 550 nm thick of PMMA in order to conduct the transmission spectrum measurements and to study the coupling effect of the bottom layer gold disks to the top layer gold nanoholes. The lateral and vertical dimensions of nanostructures were characterized by SEM conducted on an FEI Sirion SEM and tapping mode AFM performed on a Veeco Dimension 3100 AFM with a NanoScope IVa controller, respectively. The patterned substrate was cleaned in UV ozone for 20 min, rinsed with

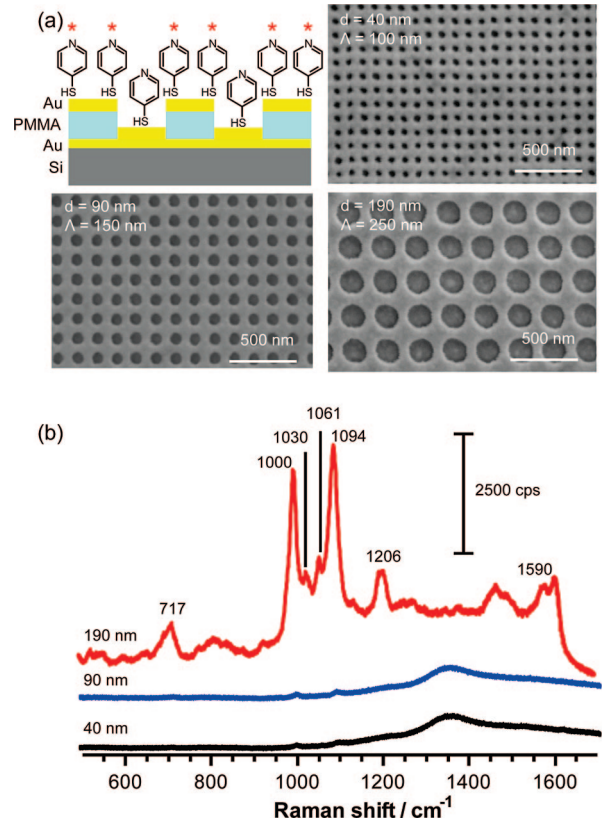

Figure 1. (a) Schematic of side view of gold thin film with nanoholes and a physically separated layer of isolated gold disks at the bottom of the well. 4-MP molecules adsorbed on the surface with an asterisk illustrate where the local electromagnetic field is enhanced. SEM images of three gold nanohole arrays with diameters of 40, 90, and 190 nm and the gratings of 100, 150, and 250 nm, respectively. The thickness of gold films is 50 nm. The depth of wells is ~100 nm measured by tapping mode AFM. (b) SERS spectra of 4-MP adsorbed on 3 gold nanohole arrays with different diameters excited by a 785 nm laser.

18.2 MΩ cm^{-1} deionized (DI) water, dried with a stream of nitrogen, and immersed in a 3 mM 4-mecaptopyridine (4-MP) aqueous solution for 3 h to form a self-assembled monolayer. Raman spectroscopy was conducted using a Renishaw InVia Raman spectrometer attached to a Leica DMLM upright microscope. A 50× (N.A. = 0.8) objective was used to focus the laser on a nanostructured array and to collect the scattering light from the sample surface. The 785 nm near-infrared laser line and the 514 nm visible laser line were used to irradiate the surface. Normal incidence transmission spectroscopy was accomplished under the white light Köhler illumination condition using a 100× (N.A. = 0.8) objective with the holographic filters removed.

4-MP has been widely used as a probe molecule for SERS study because it has a large scattering cross section and forms a self-assembled monolayer on metal surfaces comparable to alkane thiols.[19,35–39] The vibration band in 4-MP originates from the ring breathing mode, coupled with the C−S stretching, shifts the wavenumber of solid 4-MP from 1105 cm^{-1} [35,36,39] to a lower wavenumber of 1094 cm^{-1} when 4-MP is adsorbed on a gold surface via sulfur atom.[19,35,37,39] Therefore, the intensity of the band at 1094 cm^{-1} was used as an indicator for the enhancement on different nanostruc-

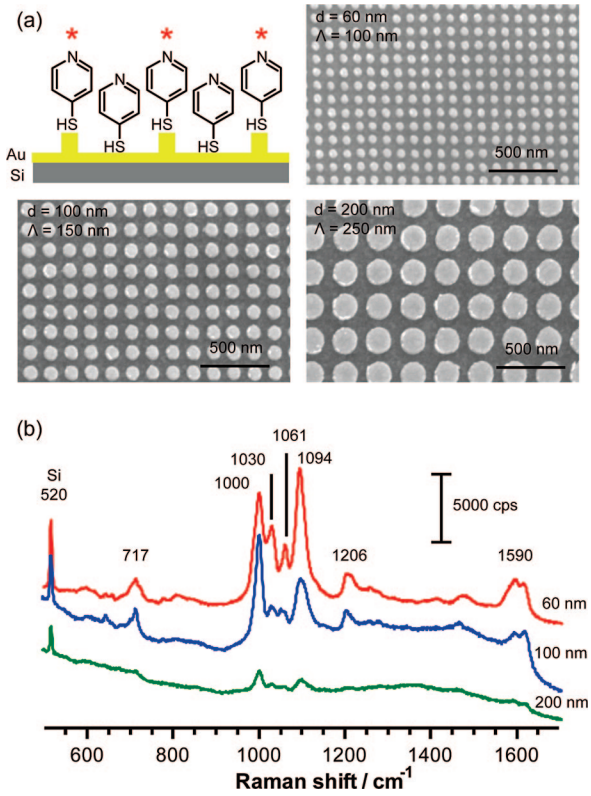

Figure 2. (a) Schematic of side view of gold nanodisks and 4-MP adsorbed on the surface. Molecules marked with an asterisk illustrate where the local electromagnetic field is enhanced. SEM images of 3 Au nanodisks with the diameters of 60, 100, and 200 nm and the gratings of 100, 150, and 250 nm, respectively. The heights of all nanodisks are 50 nm measured by tapping mode AFM. (b) SERS spectra of 4-MP adsorbed on 3 Au nanodisk arrays with different diameters exicted by a 785 nm laser.

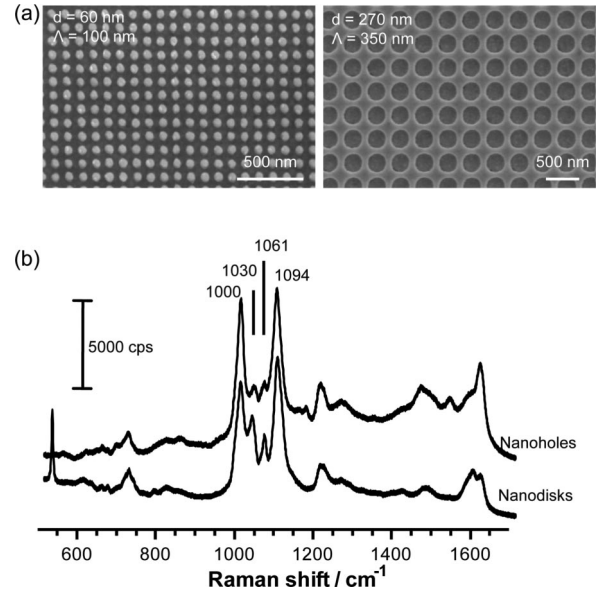

Figure 3. (a) SEM images of a gold nanohole array with a 270 nm diameter and an 80 nm edge-to-edge distance in comparison to a nanodisk array with a 40 nm diameter and a 60 nm edge-to-edge distance. (b) SERS spectra of 4-MP adsorbed on the nanohole and nanodisk arrays excited by a 785 nm laser.

tured surfaces. In Figure 1, we show that increasing the diameter of nanoholes from 40 to 90 to 190 nm while maintaining the same edge-to-edge distance between holes (~60 nm) dramatically increases the intensity of the band at 1094 cm^{-1}. The intensity is even greater when the size of the nanoholes are further increased to 200−425 nm and the edge-to-edge distance of nanoholes is kept between 80−125 nm (as shown in Table 1 for samples H_D, H_E, and H_F, Supporting Information). For similar nanohole diameters about 100 nm, increasing the nanohole edge-to-edge distance from 100 to 200 nm results in an attenuation of the 1094 cm^{-1} band intensity (see samples H_G, H_H, and H_I in Table 1, Supporting Information). The decrease of the SERS intensity as increasing nanohole spacing is in agreement with the previous study of SERS on gold nanohole arrays because of the red shifts of transmission spectra related to LSPR.[33]

In parallel, we also studied the SERS on nanodisk arrays with similar diameters and square grid spacings as the nanohole arrays. Figure 2 shows the SERS spectra of 4-MP adsorbed on nanodisk arrays with diameters and edge-to-edge distances comparable to those in the nanohole arrays. It is clearly shown that the 1094 cm^{-1} band intensity decreases as the diameters of the nanodisks are increased, demonstrating an inverted size-dependence of SERS on nanohole and nanodisk arrays. The highest intensity of SERS spectra obtained from gold nanodisk arrays had a 60 nm diameter and 40 nm edge-to-edge distance. The same enhancement can also be achieved using nanohole arrays with much larger hole diameters (270−425 nm) and edge-to-edge distance (80−125 nm). Figure 3 shows similar SERS intensities obtained from the different size nanodisk and nanohole arrays. Like nanohole arrays, the intensity of band 1094 cm^{-1} decreases as the edge-to-edge distance between nanodisks increases, which is consistent with the previous investigations.[29]

It has been well-documented that SERS results from two effects, electromagnetic field enhancement caused by LSPR associated with metallic nanostructures and chemical enhancement caused by resonance Raman-like interaction between the metallic nanostructure and the adsorbate. Most of the electromagnetic models consider a molecule as a polarizable point dipole that is localized close to a metallic sphere or spheroid. In this case, the overall gain G_{SERS} is approximately equal to the product of the gain at the laser angular frequency $g(\omega_{exc})$ and that at the Raman angular frequency $g(\omega_{RS})$. According to this model, large SERS signals are expected when both the frequency of the incident laser and the scattered Raman electromagnetic field approach the resonance frequency of LSPR. Further theoretical analysis predicts that the maximum SERS effect occurs when the LSPR wavelength, λ_{LSPR}, is equal to half the summation of the excitation (λ_{exc}) and the Raman scattering (λ_{RS}) wavelengths; that is, $\lambda_{LSPR} = {}^1/_2(\lambda_{exc} + \lambda_{RS})$.[40] This prediction has been verified by experiments, such as plasmon-sampled SERS (PS-SERS)[30,32] and wavelength-scanned SERS (WS-SERS).[41]

In our experiments, the excitation wavelength is 785 nm, and the Stokes Raman scattering wavelength corresponding

to the band 1094 cm^{-1} is 859 nm, which means that the maximum SERS effect can be achieved if the LSPR wavelength approaches 822 nm. When we used a 514 nm laser as the excitation source, no SERS signal was observed on either nanohole or nanodisk arrays. The maximum SERS effect would be achieved if the LSPR wavelength is close to 530 nm for the excitation wavelength of 514 nm and the Raman scattering wavelength of 545 nm (band 1094 cm^{-1}). These results imply that the LSPR wavelengths of nanodisk and nanohole arrays, which exhibit strong intensities of SERS excited using a 785 nm laser, are in the regime of near-infrared.

In order to elucidate the dependence of LSPR on the structure of nanohole arrays and the correlation between LSPR and SERS, we fabricated a set of nanohole arrays on ITO glass. The glass substrate allows both transmission and SERS spectra to be obtained from the same nanohole array. Since the transmission properties are sensitive to the nature of the dielectrical medium at the gold surface, the transmission spectra were taken on clean nanohole arrays prior to the SERS measurements. Figure 4 shows the SEM images, the SERS spectra of 4-MP, and the transmission spectra of four nanohole arrays with the diameters of 190, 290, 370, and 520 nm and the gratings of 300, 400, 500, and 600 nm, respectively. The intensities of the band 1094 cm^{-1} increase as diameter increases from 190 to 370 nm. However, this peak intensity appears to reach a maximum and decreases when the diameter of nanholes is further increased to 520 nm. The normal incidence transmission spectra taken of the nanohole arrays show the transmission peaks are broader and even split into two peaks as the diameters of nanoholes are increased from 190 to 520 nm. The transmission spectra are well-fitted by two peaks in each spectrum as shown in Figure 4e. The lower fitted peaks are at 662, 687, 715, and 696 nm and the higher fitted peaks are at 703, 733, 790, and 803 nm for the nanohole arrays with the diameters of 190, 290, 370, and 520 nm respectively. From the dependence of SERS effect on nanohole arrays and the shifted trend of lower fitted peaks, we believe that the lower fitted peak might be associated with LSPR of nanohole arrays. The experimental[13] and theoretical[12] studies of the optical properties of individual nanoholes show that the peaks of the elastic scattering spectra and the dipolar optical absorption spectra of individual nanoholes are red shifts as increasing nanohole diameter.[13] Recently, Rogers and co-workers[42] have shown that, in normal incidence transmission mode, such created nanohole structures, or so-called quasi-3D plasmonic crystals, exhibit strong spatial and wavelength dependent intensity modulations involving absorptive, diffractive, and plasmonic effects. They demonstrated that certain features in the transmission spectra of these nanostructures are associated, at least partly, with LSPR on the rims of the nanoholes in the upper gold film, as well as in the lower metal disks. In both their experimental and their theoretical transmission spectra of a nanostrusture with nanohole diameters of ~420 nm, depths of ~350 nm, and center-to-center spacings of ~720 nm, one peak around 883 nm is associated with LSPR behavior in the rims of the

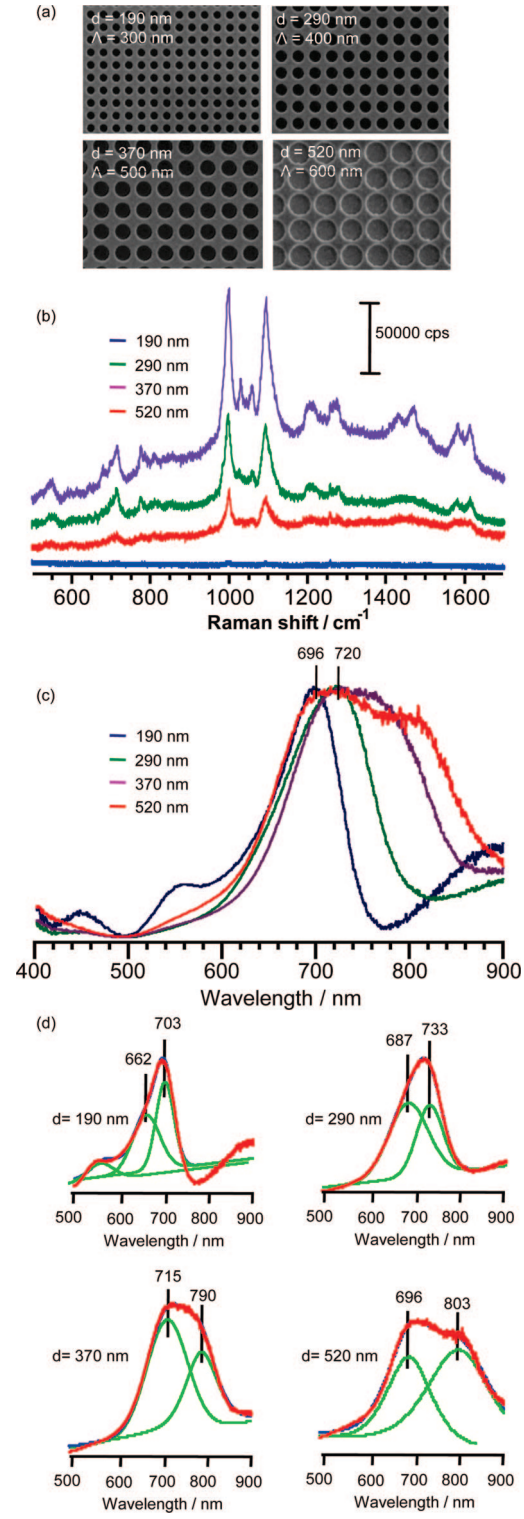

Figure 4. (a) SEM images of gold nanohole arrays with diameters from 190 to 520 nm while the edge-to-edge distance was maintained about 100 nm. These nanohole arrays were fabricated by EBL on an ITO substrate with the PMMA thickness of 550 nm and uniformly coated 50 nm gold thin film. The depth of nanoholes is ~550 nm measured by tapping mode AFM. (b) SERS spectra of 4-MP adsorbed on the nanohole arrays excited by a 785 nm laser. (c) Normalized normal incidence transmission spectra of gold nanohole arrays. (d) Fitted transmission spectra of gold nanohole arrays.

nanoholes near the air/gold interface, while another peak around 1138 nm is associated with LSPR at the gold/polymer

interface at the bottom of the wells. Their theoretical calculation also showed that the intensity of the electromagnetic field at the gold/polymer interface extends vertically up to the hole opening, indicating strong coupling between the disks and the holes. The upper limit of the transmission spectrum is approximately 900 nm on our instrument. Some of the nanohole structures created in this work have similar hole diameters but smaller center-to-center spacings and larger well depths. This may cause the peak around 883 nm[42] to shift to lower wavelength as shown in this work. We also found that the SERS signals were much stronger when the distance between the upper gold nanoholes and the lower gold disks were increased from ~100 nm to ~550 nm. In the future, quantitative computational electrodynamics modeling should be conducted to provide a more thorough understanding of SERS behavior and its relationship to LSPR of nanohole structures.

For nanodisks, the extinction spectrum is dominated by a dipolar mode, whose frequency depends on the particle size and space due to retardation effects in the intraparticle electromagnetic interaction.[43] The LSPR wavelength of a pair of nanoparticles exhibits a red shift when the interparticle distance decreases and the polarization of the incident light is parallel to the interparticle axis, while blue shifting occurs when the polarization is perpendicular to the axis.[44] When the interparticle distance is comparable with the wavelength of light, electromagnetic coupling between nanoparticles can lead to more complex behavior. Computational modeling shows that, with in-plane polarization, a decrease in interparticle distance yields a LSPR red shift for small separation but a blue shift for large separation (>100 nm).[45] In our experiment, the incident light is polarized in the direction parallel to the edge of square lattice. When the distance between nanodisks is decreased, the LSPR wavelength is expected to shift to longer wavelengths, resulting in stronger SERS signals (such as samples D_D, D_E, and D_F in Table 1, Supporting Information).

In order to directly compare the SERS effect on nanodisk and nanohole arrays, we calculated the enhancement factor $EF = I_{surf}N_{bulk}/I_{bulk}N_{surf}$, where I_{surf} and I_{bulk} are the intensities of the band 1094 cm^{-1} from the SERS substrates and solid sample, respectively, and N_{surf} and N_{bulk} are the number of molecules on the surface in the area illuminated by the light and in the bulk with the volume of illumination, respectively (details of calculations are given as Supporting Information). The highest EF of 4.2×10^5 was obtained on the nanohole array with the diameter of 370 nm, the grating of 500 nm, and the well depth of 550 nm. This EF is 2 orders of magnitude higher than the highest EF of 1.3×10^3 obtained on the nanodisk array with the diameter of 60 nm and the grating of 100 nm. There is a wide range of hole diameters and grating parameters for nanohole arrays to achieve high enhancement factor. The diameters of 300−500 nm and the edge-to-edge distance of ~100 nm for nanohole structures make the fabrication much easier than the very small dimensions required for nanodisk arrays. Alternative fast and cost-effective nanofabrication methods, such as soft lithography, can be employed.

In summary, it has been shown that regular gold nanohole arrays exhibit strong SERS effect which can be manipulated by controlling the diameter of holes and the distance between holes. The SERS effect can be attributed to varying degrees of electromagnetic coupling between holes, which determines the wavelength of LPSR associated with the nanohole arrays. In contrast to nanohole arrays, nanodisk arrays exhibit stronger SERS effect as the diameter of nanodisks decreases. The dependence of SERS effect observed from different dimensions of nanohole and nanodisk arrays results from the difference in the LSPR modes that are most efficiently excited for nanohole and nanodisk arrays. The large tolerance on dimensions and the empty space confined by nanoholes suggest promise for their use as a functional component in sensing, spectroscopy, and photonic devices.

Acknowledgment. This work was conducted at the Nanotech User Facility at the University of Washington, a member of the National Nanotechnology Infrastructure Network (NNIN) supported by the NSF.

Supporting Information Available: The dimensions of nanohole and nanodisk arrays and calculations of the enhancement factor. This material is available free of charge via the Internet at http://pubs.acs.org.

References

(1) Barnes, W. L.; Dereux, A.; Ebbesen, T. W. *Nature* **2003**, *424*, 824–830.
(2) Gordon, R.; Brolo, A. G.; McFarland, A. D.; Rajora, A.; Leathem, B.; Kavanagh, K. L. *Phys. Rev. Lett.* **2004**, *92*, 037401.
(3) Ebbesen, T. W.; Lezec, H. J.; Ghaemi, H. F.; Thio, T.; Wolff, P. A. *Nature* **1998**, *391*, 667–669.
(4) Gao, H. W.; Henzie, J.; Odom, T. W. *Nano. Lett.* **2006**, *9*, 2104–2108.
(5) Altewischer, E.; van Exter, M. P.; Woerdman, J. P. *Nature* **2002**, *418*, 304–306.
(6) Degiron, A.; Lezec, H. J.; Barnes, W. L.; Ebbesen, T. W. *Appl. Phys. Lett.* **2002**, *81*, 4327–4329.
(7) Thio, T.; Ghaemi, H. F.; Lezec, H. J.; Wolff, P. A.; Ebbesen, T. W. *J. Opt. Soc. Am. B* **1999**, *16*, 1743–1748.
(8) Wannemacher, R. *Opt. Commun.* **2001**, *195*, 107–118.
(9) Tan, W.-C.; Preist, T. W.; Sambles, R. J. *Phys. Rev. B* **2000**, *62*, 11134–11138.
(10) Shuford, K. L.; Ratner, M. A.; Gray, S. K.; Schatz, G. C. *J. Comput. Theor. Nanosci.* **2007**, *4*, 239–246.
(11) Prikulis, J.; Hanarp, P.; Olofsson, L.; Sutherland, D.; Käll, M. *Nano. Lett.* **2004**, *4*, 1003–1007.
(12) Park, T.-H.; Mirin, N.; Lassiter, J. B.; Nehl, C. L.; Halas, N. J.; Nordlander, P. *ACS Nano* **2008**, *2*, 25–32.
(13) Rindzevicius, T.; Alaverdyan, Y.; Sepulveda, B.; Pakizeh, T.; Käll, M.; Hillenbrand, R.; Aizpurua, J.; García de Abajo, J. F. *J. Phys. Chem. C.* **2007**, *111*, 1207–1212.
(14) Dahlin, A.; Zäch, M.; Rindzevicius, T.; Käll, M.; Sutherland, D. S.; Höök, F. *J. Am. Chem. Soc.* **2005**, *127*, 5043–5048.
(15) Sonnichsen, C.; Duch, A. C.; Steininger, G.; Koch, M.; von Plessen, G.; Feldmann, J. *Appl. Phys. Lett.* **2000**, *76*, 140–142.
(16) Rindzevicius, T.; Alaverdyan, Y.; Dahlin, A.; Höök, F.; Sutherland, D. S.; Käll, M. *Nano. Lett.* **2005**, *5*, 2335–2339.
(17) De Leebeeck, A.; Swaroop, L. K.; de Lange, V.; Sinton, D.; Gordon, R.; Brolo, A. G. *Anal. Chem.* **2007**, *79*, 4094–4100.
(18) Brolo, A. G.; Gordon, R.; Leathem, B.; Kavanagh, K. L. *Langmuir* **2004**, *20*, 4813–4815.
(19) McLellan, J. M.; Xiong, Y. J.; Hu, M.; Xia, Y. N. *Chem. Phys. Lett.* **2006**, *417*, 230–234.
(20) Wiley, B. J.; Im, S. H.; Li, Z. Y.; McLellan, J. M.; Siekkinen, A.; Xia, Y. N. *J. Phys. Chem. B* **2006**, *110*, 15666–15675.
(21) Hulteen, J. C.; Van Duyne, R. P. *J. Vac. Sci. Technol. A* **1995**, *13*, 1553–1558.

(22) Hanarp, P.; Käll, M.; Sutherland, D. S. *J. Phys. Chem. B* **2003**, *107*, 57685772.
(23) Zheng, Y. B.; Juluri, B. K.; Mao, X. L.; Walker, T. R.; Huang, T. J. *J. Appl. Phys.* **2008**, *103*, 014308.
(24) Haynes, C. L.; McFarland, A. D.; Zhao, L. L.; Van Duyne, R. P.; Schatz, G. C. *J. Phys. Chem. B* **2003**, *107*, 7337–7342.
(25) Stuart, D. A.; Haes, A. J.; Yonzon, C. R.; Hicks, E. M.; Van Duyne, R. P. *IEE Proc.-Nanobiotechnol.* **2005**, *152*, 13–32.
(26) García de Abajo, F. J. *Rev. Mod. Phys.* **2007**, *79*, 1267–1290.
(27) Tian, Z. Q.; Ren, B.; Wu, D. Y. *J. Phys. Chem. B* **2002**, *106*, 9463–9483.
(28) Félidj, N.; Aubard, J.; Lévi, G. *Appl. Phys. Lett.* **2003**, *82*, 3095–3097.
(29) Gunnarsson, L.; Bjerneld, E. J.; Xu, H.; Petronis, S.; Kasemo, B.; Käll, M. *Appl. Phys. Lett.* **2001**, *78*, 802–804.
(30) Grand, J.; de la Chapelle, M. L.; Bijeon, L.-J.; Adam, P.-M.; Vial, A.; Royer, P. *Phys. Rev. B* **2005**, *72*, 033407.
(31) De Jesus, M. A.; Giesfeldt, K. S.; ORAN, J. M.; Abu-Hatab, N. A.; Lavrik, N. V.; Sepaniak, M. J. *Appl. Spectrosc.* **2005**, *59*, 1501–1508.
(32) Haynes, C. L.; Van Duyne, R. P. *J. Phys. Chem. B* **2003**, *107*, 7426–7433.
(33) Brolo, A. G.; Arctander, E.; Gordon, R.; Leathem, B.; Kavanagh, K. L. *Nano. Lett.* **2004**, *4*, 2015–2018.
(34) Reilly III, T. H.; Chang, S.-H.; Corbman, J. D.; Schatz, G. C.; Rowlen, K. L. *J. Phys. Chem. C* **2007**, *111*1689–1694.
(35) Hu, J. W.; Zhao, B.; Xu, W. Q.; Li, B. F.; Fan, Y. G. *Spectrochim. Acta, Part A* **2002**, *58*, 2827–2834.
(36) Wang, Z. J.; Rothberg, L. J. *J. Phys. Chem. B* **2005**, *109*, 3387–3391.
(37) Yu, H. Z.; Xia, N.; Liu, Z. F. *Anal. Chem.* **1999**, *71*, 1354–1358.
(38) Wang, Z.; Rothberg, L. J. *J. Chem. Phys. B* **2005**, *109*, 3387–3391.
(39) Bryant, M. A.; Joa, S. L.; Pemberton, J. E. *Langmuir* **1992**, *8*, 753–756.
(40) Félidj, N.; Aubard, J.; Lévi, G.; Krenn, J. R.; Salerno, G.; Schider, G.; Lamprecht, B.; Leitner, A.; Aussengg, F. R. *Phys. Rev. B* **2002**, *65*, 075419.
(41) McFarland, A. D.; Young, M. A.; Dieringer, J. A.; Van Duyne, R. P. *J. Phys. Chem. B* **2005**, *109*, 11279.
(42) Stewart, M. E.; Mack, N. H.; Malyarchuk, V.; Soares, J. A. N. T.; Lee, T.-W.; Gray, S. K.; Nuzzo, R. G.; Rogers, J. A. *Proc. Natl. Acad. Sci. U.S.A.* **2006**, *103* (46), 17143–17148.
(43) Kottmann, J. P.; Martin, O. J. F. *Opt. Lett.* **2001**, *26* (14), 1096–1098.
(44) Rechberger, W.; Hohenau, A.; Leitner, A.; Krenn, J. R.; Lamprecht, B.; Aussengg, F. R. *Opt. Commun.* **2003**, *220*, 137–141.
(45) Zhao, L.; Kelly, K. L.; Schatz, G. C. *J. Phys. Chem. B* **2003**, *107*, 7343–7350.

NL0806163